ELSEVIER

Dust transport in photoelectron layers and the formation of dust ponds on Eros

Joshua E. Colwell [a,*], Amanda A.S. Gulbis [b], Mihály Horányi [a], Scott Robertson [c]

[a] *Laboratory for Atmospheric and Space Physics, University of Colorado, Boulder, CO 80309-0392, USA*
[b] *Department of Earth, Atmospheric, and Planetary Sciences, Massachusetts Institute of Technology, Cambridge, MA 02139, USA*
[c] *Center for Integrated Plasma Studies, University of Colorado, Boulder, CO 80309-0390, USA*

Abstract

We investigate the electrostatic transport of charged dust in the photoelectron layer over the dayside surface of an asteroid. Micron-sized dust particles may be levitated above the surface in the photoelectron layer. Horizontal transport within the layer can then lead to net deposition of dust into shadowed regions where the electric field due to the photoelectron layer disappears. We apply a 2D numerical model simulating charged dust dynamics in the near-surface daytime plasma environment of Asteroid 433 Eros to the formation of dust deposits in craters. We find that dust tends to collect in craters and regions of shadow. This electrostatic dust transport mechanism may contribute to the formation of smooth dust ponds observed by the NEAR-Shoemaker spacecraft at Eros. The size distribution of transported dust depends on the particle density and work function, and the work function of the surface and solar wind electron temperature and density. With reasonable values for these parameters, μm-sized and smaller particles are levitated at Eros. Micrometeoroid bombardment is not a sufficient source mechanism for electrostatic transport to create the Eros dust ponds. Laboratory measurements of dust in a plasma sheath show that dust launched off the surface by direct electrostatic levitation can provide a sufficient source for transport to produce the observed Eros ponds.
© 2004 Elsevier Inc. All rights reserved.

Keywords: Eros; Surfaces, asteroids; Regoliths

1. Introduction

Dusty regoliths are produced on the surfaces of virtually all airless bodies in the Solar System through ongoing bombardment by the interplanetary micrometeoroid flux. If these dust particles become charged, they may be transported across the surface by electrostatic interactions with the near-surface plasma environment. For example, lunar electrostatic dust dynamics are believed to be responsible for several observed dust phenomena (Zook et al., 1995; Zook and McCoy, 1991; Berg et al., 1974, 1976; Rennilson and Criswell, 1974; McCoy and Criswell, 1973). The spokes in Saturn's rings are most likely clouds of particles electrostatically levitated from the surfaces of larger bodies in the rings (Nitter et al., 1998; Goertz, 1989). In addition, electrostatic dust transport processes have been proposed on the surface of Mercury (Ip, 1986) and comets (Mendis et al., 1981).

The surface of Asteroid 433 Eros reveals a complex regolith in high resolution images taken by the NEAR-Shoemaker spacecraft (e.g., Veverka et al., 2000; Cheng et al., 2001; Kerr, 2001). Smooth deposits, or "ponds" were observed in craters ranging in size from 20 to 300 m in diameter (Veverka et al., 2001). The deposits are smooth down to 1.2 cm per pixel resolution indicating they are composed of particles significantly smaller than 1 cm (Robinson et al., 2001). The colors of the pond material, large boulders, and the background landscape are nearly indistinguishable (Veverka et al., 2001), though the ponds are slightly bluer in the visible than the surrounding terrain. The homogeneity of the surface colors can be explained by a layer of fine dust

---

over the surface and is consistent with the ponds being composed of dust. The small color differences of the ponds can also be explained by a size distribution of grains $\ll$ 50 µm (Robinson et al., 2001).

The mapped distributions of larger ponds correspond well with local regions of particularly long terminator durations, and there is an excellent correlation between ponds and low gravity areas (Robinson et al., 2001). Of the 255 large ponds (> 30 m diameter) 231 are located within 30° of the equator. These areas therefore also see the Sun rise and set, a factor that is required if terminator electric fields play a role in their formation. The observed characteristics of the Eros ponds require a mechanism that separates the fine fraction of regolith and a mechanism to concentrate particles in the depression that is most efficient along the equatorial belt. Global ejecta blanketing events can be ruled out by the correlation between pond depth and crater diameter.

Electrostatic dust levitation and transport has been proposed as a possible explanation for the observed dusty features on Eros (Cheng et al., 2002; Robinson et al., 2001; Pieters, 2001; Tepliczky and Kereszturi, 2002). This explanation was anticipated by Lee (1996) who recognized that levitated charged dust grains over asteroids could be transported to "smooth, flat, and/or perennially shaded areas, or where the particles become physically trapped, e.g., in topographic asperities and/or lows in dynamic height." Pond-like deposits have been observed in topographic depressions that are not craters (Veverka et al., 2001), consistent with the electrostatic model. The boundary between the smooth, flat, pond surface and crater walls can be quite abrupt (Robinson et al., 2001), and these craters "do not show… evidence of downslope movement on the crater walls" (Veverka et al., 2001). These observations are consistent with electrostatic transport of dust playing a role in the formation of the pond deposits. Other mechanisms that may be responsible for part or all of the formation of ponded deposits on Eros include seismic shaking (Cheng et al., 2002) and size sorting through evaporative processes (Kareev et al., 2002). We present results on the transport of charged dust near the surface of Eros and apply it to the question of the formation of the ponded deposits.

This work provides a numerical approach to the analysis of dust levitation and subsequent redistribution, and concentrates on the conditions at Asteroid 433 Eros. We investigate the role of electrostatic processes in redistributing material on the surface of Eros and producing some of the unusual features of its regolith, and we present a numerical model that simulates dust transport in a photoelectron sheath above a surface on Eros. A description of electrostatic dust levitation on asteroids is presented in Section 2. Our numerical model for transport on Eros is described in Section 3, and the results are presented in Section 4. Section 5 provides a discussion and conclusions. Our numerical simulations demonstrate that this mechanism may play an important role in the formation of the dust ponds seen at Eros.

2. Electrostatic dust levitation

2.1. Sheath and dust charging processes

The primary charging currents for the sunlit side of an asteroid are solar wind electrons, solar wind ions, and photoemission. On a sunlit, airless surface in interplanetary space, where the plasma density is that of the tenuous solar wind, photoelectric charging usually exceeds plasma charging. In the absence of other charging processes these surfaces become positively charged. The floating potential is dependent on the energy of the incoming photons and the photoelectric work function of the surface material. In equilibrium, the surface potential becomes positive enough to return emitted photoelectrons to the surface. These outbound and inbound electrons form a photoelectron sheath, or layer, above the surface. The photoelectrons in the sheath generate a vertical electric field which acts to return negatively charged particles to the surface and accelerate positively charged particles away from the surface.

Dust particles resting on the surface may become positively charged due to photoemission. If positively charged particles detach from the surface, they can thus be levitated in the photoelectron sheath. Conversely, dust particles that collect enough photoelectrons in the sheath to become negatively charged are accelerated down to the positively charged surface. When a particle leaves the surface the current of photoelectrons to the particle exceeds the current of photoemitted electrons and it can attain a negative charge as it passes through the photoelectron layer. If its initial velocity is high enough it will make it through the layer and attain a positive charge due to its own photoemission, making it possible for the particle to be stably supported by the upward electric field in the sheath. If, on the other hand, the particle spends too much time in the sheath, it will be negatively charged and accelerated toward the surface. The dynamics of a charged dust particle near the surface of an asteroid or other airless planetary body thus depend on the local plasma environment, the gravity of the body, and the variable charge of the grain. The levitation of dust particles in plasma sheaths has been studied numerically (e.g., Nitetal et al., 1994, 1998) and experimentally (Doe et al., 1994; Arnas et al., 1999; Robertson et al., 2003).

Over small spatial scales, such as along the terminator of a rough surface, UV illuminated regions are adjacent to unilluminated regions. The photoemission from the illuminated regions leads to differential charging. Therefore, horizontal electric fields can occur in a photoelectron sheath in addition to the existing vertical field. Dust particles released from the surface may be transported across the surface in these fields. Also, if particles have any horizontal velocity when they enter the sheath, or if there are enough dust particles in the sheath to interact with each other electrically, then horizontal transport of dust will occur, with a deposition of dust where the topography changes or the electric field strength is reduced. The electric field may be greatly

reduced or vanish in shadowed regions of a photoelectron sheath.

Such electrostatic interactions are likely the source of the observed dust dynamics on the Moon (e.g., Pelizzari and Criswell, 1978; Criswell, 1972, 1973; Gold, 1955). Like the Moon, asteroids are primarily unmagnetized bodies in the Solar System that lack atmospheres. Asteroids are typically located farther from the Sun than the Moon, so the corresponding solar wind and photoemission currents to an asteroid surface are typically smaller than at the lunar surface. However, the gravitational force on an asteroid such as 433 Eros is roughly two orders of magnitude lower than on the Moon. Depending on the properties of the plasma environment, dust particles may levitate in the photoelectron sheath above the sunlit surface of an asteroid.

We next investigate the general properties of single particle dynamics in a photoelectron sheath on Eros. We note that a similar phenomenon is possible in the solar wind plasma sheath on the night side of an asteroid. Furthermore at the terminator the combination of photoelectron currents and the solar wind creates a more complex charging environment. In this paper we restrict our study to the dayside photoelectron layer.

2.2. Single particle dust charging

The charge on a particle in a photoelectron sheath is determined by the currents due to collection of photoelectrons in the sheath, I_e, and the emission of photoelectrons from the grain itself, I_{pe}. Particles are also subject to additional currents from the solar wind electrons and ions. In the solar wind particles attain a positive charge due to photoemission, which is moderated by the collection of solar wind electrons. We can therefore neglect solar wind ions and only consider current due to solar wind electrons, I_{sw}. The charging equation for a dust particle above the surface is then given by

$$dQ_d/dt = I_{pe} - I_e - I_{sw}, \tag{1}$$

where Q_d is the dust particle charge.

The current of photoelectrons to the particle is given by (Havnes et al., 1987):

$$I_e = \pi r_d^2 e n_{pe} \sqrt{\frac{8k_B T_{pe}}{\pi m_e}} \exp\left(\frac{e\phi_d}{k_B T_{pe}}\right), \quad \phi_d \leqslant 0,$$

$$I_e = \pi r_d^2 e n_{pe} \sqrt{\frac{8k_B T_{pe}}{\pi m_e}} \left(1 + \frac{e\phi_d}{k_B T_{pe}}\right), \quad \phi_d > 0, \tag{2}$$

where ϕ_d is the potential of the particle, r_d is the particle radius, e is the electron charge, k_B is the Boltzmann constant, m_e is the electron mass, T_{pe} is the photoelectron temperature, and n_{pe} is the photoelectron density in the sheath.

The photoelectron density in the sheath is determined by the photoelectron current away from the surface and the resulting positive surface potential. The photoelectron current is determined by the flux of solar photons with sufficient energy to knock electrons off the surface, $F(\lambda < \lambda_1)$, and the quantum efficiency of photoemission from the material, $\chi(\lambda)$:

$$I_{ph0} = \int_0^{\lambda_1} F(\lambda)\chi(\lambda)\, d\lambda, \tag{3}$$

where $\lambda_1 \sim 200$ nm is the longest wavelength photon capable of producing a photoelectron from a surface with a typical work function, $W \sim 5$ eV (e.g., Sternovsky et al., 2002). Both F and χ are strongly dependent on wavelength, so χ should not be pulled outside the integral. Rather than adopt a functional form for χ and a value for λ_1 and evaluate the integral in Eq. (3), we will assume that the dust and surface of Eros have the same photoemissive properties as the lunar regolith, for which $\chi(\lambda)$ has been directly measured. The resulting photocurrent at a distance d (in AU) from the Sun is $I_{ph0} = 2.8 \times 10^9/d^2$ electrons/(cm² s) (Willis et al., 1973). The photoelectron density at the surface is then given by

$$n_{pe,0} = 2I_{ph0}\sin(i_s)/\upsilon_{pe}, \tag{4}$$

where υ_{pe} is the average photoelectron emission velocity and i_s is the solar elevation angle above the horizon. We take the average photoelectron temperature of $k_B T_{pe} = 2.2$ eV as measured for lunar regolith (Willis et al., 1973), giving $\upsilon_{pe} = 8.8 \times 10^7$ cm/s. Assuming a Maxwellian distribution of photoelectron energies, the photoelectron density in the sheath as a function of height above the surface is given by Grard and Tunaley (1971):

$$n_{pe} = n_{pe,0}\left(1 + \frac{z}{\sqrt{2}\lambda_D}\right)^{-2}, \tag{5}$$

where z is the height of the grain above the surface, and

$$\lambda_D = \sqrt{\frac{k_B T_{pe}}{4\pi n_{pe,0} e^2}} \tag{6}$$

is the Debye length at the surface. The photoelectron energy distribution cannot be a true Maxwellian because there must be an upper limit to the photoelectron energy. However, more detailed solutions of the charge distribution, including particle-in-cell calculations (Sickafoose et al., 2001) and solutions of Poisson's equation including photoelectron and plasma populations (Nitter et al., 1998) give a vertical profile similar to that in Eq. (5). The solutions of Nitter et al. (1998) also show that the photoelectron layer profile does not change significantly with solar incidence angle for $i_s > 5°$. We therefore assume for simplicity that the vertical profile of the photoelectron layer has the form of Eq. (5) independent of i_s, but we only consider values of $i_s > 10°$. Also, we neglect the small contribution of solar wind electrons to the near-surface electron density in calculating the Debye length.

The photoemission current of electrons leaving a dust particle is also calculated from the flux of high energy photons from the Sun, I_{ph0}, assuming the material properties of

the particles are the same as the surface. The current of photoelectrons emitted by the grain is then given by

$$I_{pe} = \pi r_d^2 e I_{ph0}, \quad \phi_d \leqslant 0,$$

$$I_{pe} = \pi r_d^2 e I_{ph0} \exp\left(\frac{-e\phi_d}{k_B T_{pe}}\right), \quad \phi_d > 0. \tag{7}$$

The final current we consider is the collection of solar wind electrons. We assume the solar wind electron density is constant, although very close to the surface the positively charged surface should lead to a slight enhancement. The solar wind electron density is $n_{sw} \approx 5/d^2$ cm^{-3} (e.g., (Mendis et al., 1981)), or less than 10% of the photoelectron density, $n_{pe,0} = 64/d^2$ cm^{-3}, near the surface at noon (Eq. (4)). Several Debye lengths above the surface, however, collection of solar wind electrons balances the photocurrent from the particle. The current due to collection of solar wind electrons, following Eq. (2), is

$$I_{sw} = \pi r_d^2 e n_{sw} \sqrt{\frac{8 k_B T_{sw}}{\pi m_e}} \exp\left(\frac{e\phi_d}{k_B T_{sw}}\right), \quad \phi_d \leqslant 0,$$

$$I_e = \pi r_d^2 e n_{sw} \sqrt{\frac{8 k_B T_{sw}}{\pi m_e}} \left(1 + \frac{e\phi_d}{k_B T_{sw}}\right), \quad \phi_d > 0, \tag{8}$$

where the solar wind electron temperature, T_{sw}, is assumed to be 10 eV. While the actual values for n_{sw} and T_{sw} may vary considerably around the nominal values we have chosen, the solar wind electron current acts primarily in this model to prevent the grain charge from growing without bound due to photoemission when it is outside the photoelectron sheath and reasonable changes in these parameters do not qualitatively affect our results.

By setting Eq. (1) equal to zero we calculate the equilibrium dust particle potential as a function of height, where the potential is related to the charge via $Q_d = r_d \phi_d$. We use $d = 1.78$ AU, the aphelion distance of Eros, throughout the rest of this paper. The equilibrium dust particle potential with these parameters is shown in Fig. 1. Within about one Debye length of the surface the particle is negatively charged due to collection of photoelectrons in the photoelectron layer, and then reaches a positive charge at larger distances above the surface where photoemission from the particle itself dominates the current from solar wind electrons.

2.3. Electric field and dust levitation conditions

The strength of the electric field as a function of height above the surface for a Maxwellian photoelectron energy distribution, is given by (Grard and Tunaley, 1971)

$$E = 2\sqrt{2}\Phi_s \lambda_D \left(1 + \frac{z}{\sqrt{2}\lambda_D}\right)^{-1}, \tag{9}$$

where Φ_s is the floating potential of the surface. The electric field is shown in Fig. 1 for a surface with the Sun directly overhead. We calculate the surface potential by numerically
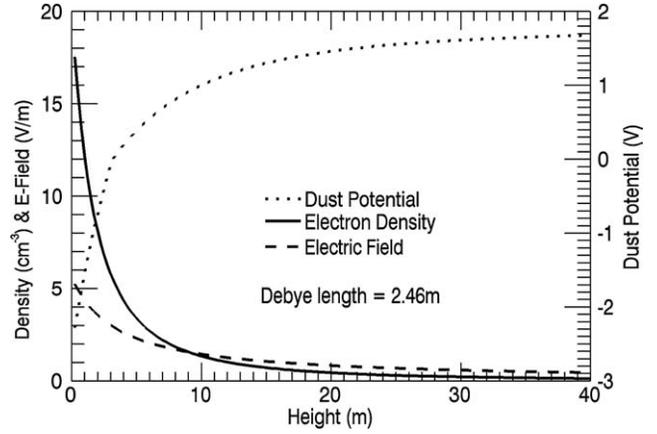

Fig. 1. Equilibrium dust particle potential as a function of height in the photoelectron layer with the charging currents described in the text. The electron density and vertical electric field strength are also shown for local solar noon on Eros. Dust particles reach an equilibrium potential of 1.78 V in the solar wind.
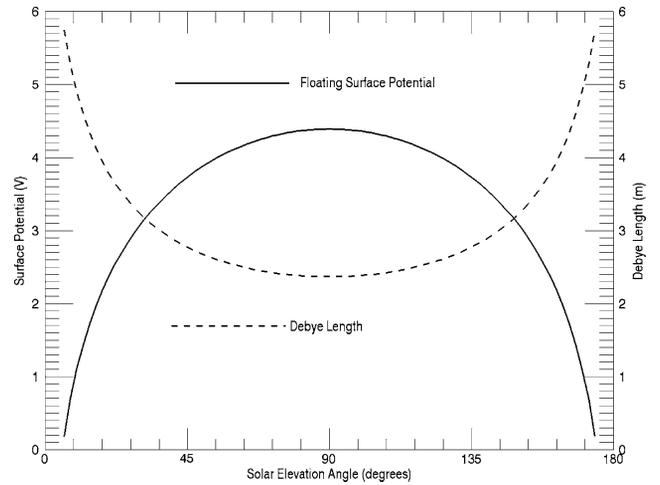

Fig. 2. Diurnal variation of the surface potential on Eros determined by the balance of photoemission from the surface and collection of solar wind electrons, and the Debye length, λ_D. Although the Debye length is roughly half as long at local noon as it is near sunset and sunrise, the stronger electric field due to the greater photoelectron density results in an effective expansion of the photoelectron layer and an increase in the levitation height for charged dust particles.

solving for the balance of the photoelectron current from the surface and the current of solar wind electrons to the surface:

$$I_{ph0} \exp\left(\frac{-e\Phi_s}{k_B T_{pe}}\right) \sin(i_s) = n_{sw} \sqrt{\frac{k_B T_{sw}}{2\pi m_e}} \left(1 + \frac{e\Phi_s}{k_B T_{sw}}\right). \tag{10}$$

The surface potential and photoelectron layer Debye length are shown in Fig. 2 as a function of solar elevation angle.

We can now determine what size particles can be levitated in the photoelectron layer. We first consider the static case of stationary particles in charge equilibrium. Solving Eqs. (3), (7), (8) for the equilibrium charge as a function of height together with the electric field as a function of height

ARTICLE IN PRESS
S0019-1035(04)00384-7/FLA AID:7523 Vol.●●●(●●●)   yicar7523   [DTD5] P.5 (1-11)
YICAR:m5 v 1.35 Prn:22/02/2005; 9:54   by:Rima p. 5

Electrostatic dust transport on Eros   5
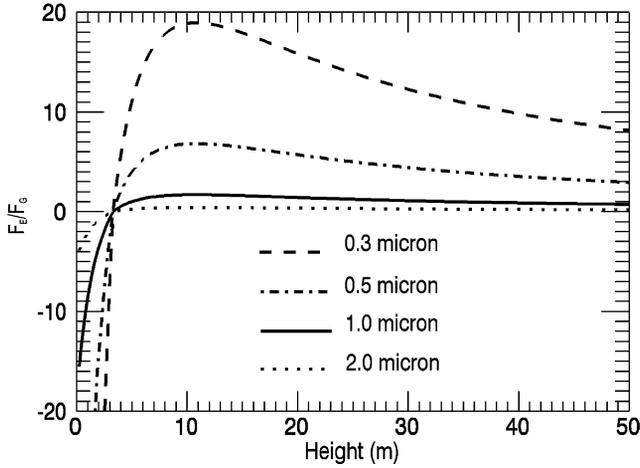
Fig. 3. The ratio of the electric force to the gravitational force acting on particles of different sizes at noon on Eros. Within one Debye length of the surface particles are negatively charged and the electric force is downward (negative in this plot). Levitation is possible when the ratio is 1. The upper equilibrium point is stable and increases in height for smaller particles. Particles larger than 1.3 μm in radius never experience an upward electric force strong enough to overcome gravity.
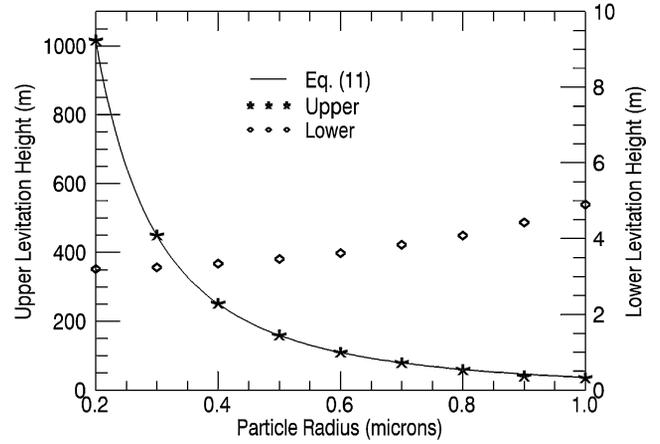

Fig. 4. Levitation heights as a function of particle size at noon on Eros. The solid line shows the value assuming the particle potential has reached its value in the solar wind (Eq. (11)) and matches the values using the calculated particle potential. The lower levitation point is unstable: a downward perturbation pushes the particle into the negative charge regime where it is accelerated to the surface, and an upward perturbation results in a stronger upward electric force, accelerating the particle further upward to the upper levitation height.

(Eq. (9)) gives the electric force as a function of height for different particle sizes (Fig. 3). Because the charge increases with height while the electric field strength declines with height, the strength of the electric force on a particle is considerably less than the value obtained by just using the equilibrium charge and the near-surface electric field strength. With the photoelectron and solar wind parameters described above, the equilibrium particle potential in the solar wind is $\phi_{eq}(z \gg \lambda_D) = 1.78$ V, $\lambda_D = 2.46$ m, and the surface electric field strength is $E_0 = 5.04$ V/m.

There are two heights at which the electric force balances the gravitational force (Fig. 3). The lower equilibrium point is unstable (Nitter et al., 1998; Robertson et al., 2003). At the upper equilibrium point, the particle potential can be assumed to have the equilibrium value of ϕ_{eq} in the solar wind. Solving the force balance for the upper levitation height we find

$$z_{eq} = \sqrt{2}\lambda_D \left(\frac{3E_0\phi_{eq}}{4\pi\rho_d g r_d^2} - 1 \right), \tag{11}$$

where g is the gravitational acceleration and ρ_d is the density of dust particles, assumed to be 3.7 g/cm^3 consistent with dense ordinary chondrites. We use the maximum local gravitational acceleration on Eros of $g = 0.55$ cm/s^2. We find the largest particle that can be stably levitated in the photoelectron layer with these parameters has a radius of 1.3 μm. However, in regions of lower surface gravity on Eros, and if the grains are less dense than the conservatively high value for ρ_d we have assumed, levitated grains will be larger than this. Also, in the presence of strong electric fields near the terminator larger particles may be temporarily levitated. The calculated upper and lower levitation heights as well the values determined from Eq. (11) are shown in Fig. 4.

2.4. Single particle dynamics

We next consider the trajectory of a particle moving over the surface of Eros under the influence of gravity and the electric force. We ignore radiation pressure and drag forces for the present model which studies short timescale dynamics of particles. The particle is not required to be in charge equilibrium, and its instantaneous charge is calculated simultaneously with its trajectory. Particles resting on the surface are likely to attain a positive charge like the surface as a whole, and this can lead to the initial electrostatic levitation of the particle. However, small individual particles may acquire significantly different dust potentials than the surface potential. For simplicity we give particles no initial net charge. They quickly attain a negative charge as they enter the photoelectron layer and become positively charged above about one Debye length (Fig. 1). Starting the particles with a positive charge on the surface would make it easier for particles with a slower initial vertical velocity to rise above the sheath, but on Eros the gravity is so weak that this is not an important consideration. We ignore any horizontal components of the electric field and assume our surface is perpendicular to the gravitational force, so the only accelerations are in the vertical direction:

$$\frac{dz}{dt} = \frac{Q_d}{m_d} E - g, \tag{12}$$

where m_d is the mass of the grain.

Integrating Eqs. (1) and (12) simultaneously produces the trajectories in Fig. 5 for particles launched at five different speeds off the surface of Eros for $r_d = 0.5$ μm. The particle launched at 0.3 m/s stays within the dense part of the photoelectron layer and therefore remains negatively charged, so both gravity and the electric force act to return it to the
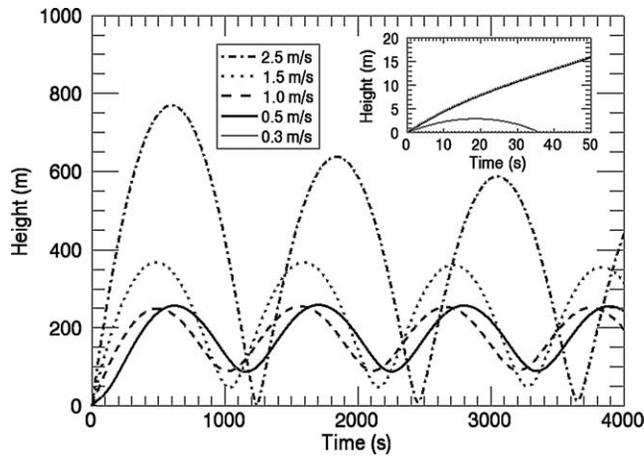
Fig. 5. Vertical position as a function of time for particles with $r_d = 0.5$ μm at solar noon on Eros, with different initial vertical velocities. All particles are accelerated up above the photoelectron layer except the particle with $v_0 = 0.3$ m/s which remains within the first Debye length of the surface and therefore remains negatively charged. This particle is returned to the surface after reaching a maximum height of 3 m, while a particle launched only slightly faster ($v_0 = 0.5$ m/s) is accelerated upward to a maximum height of 250 m. Particles launched faster than 2.5 m/s penetrate the photoelectron layer too quickly on descent to be decelerated before hitting the surface.

surface. The particle launched slightly faster, at 0.5 m/s, becomes positively charged at ∼ 5 m above the surface and is then accelerated upward to the stable levitation height for particles of this size. As the launch speed increases the initial height of the particle trajectory increases resulting in greater kinetic energy as the particle falls back toward the photoelectron layer. If this energy is too large the particle reaches the surface before the electric force reverses its motion. Consequently particles of this size with an initial velocity greater than about 2.5 m/s do not become levitated but instead penetrate the photoelectron layer and land on the surface.

This maximum launch velocity for levitation is size dependent because the charge to mass ratio is larger for smaller particles. Smaller particles can be launched at faster speeds and still be caught by the photoelectron layer and levitated. Particles on the order of 0.1 μm in radius and smaller levitate at such a large altitude above the surface of Eros that radiation pressure becomes an important perturbing force that can ultimately lead to loss of particles from the asteroid entirely.

3. Simulation of dust transport into craters

In this first work we do not include a detailed gravity and topography model of individual craters on Eros. We use a one-dimensional profile of relative surface height to model the Eros surface, and embed a model crater by placing a circular depression with a depth-to-diameter ratio of 0.25 in the center of our simulation space. We model the surface in one dimension with a length of 1 km discretized into 100 positions. We assume that the regolith is fine-grained with a size distribution of particles extending down to sub-μm particles which can be levitated in the near-surface electric fields.

Dust particles are launched from each position on the surface, one at a time, at launch angle α_0, from the surface in each direction at launch velocity v_0. The particle trajectory is simultaneously integrated in two dimensions (horizontal and vertical) with the particle charge until the grain comes into contact with the surface or a maximum time limit (10^4 s) is exceeded. The time limit is exceeded for particles that are stably levitated in the sheath, have been accelerated to escape velocity, or are on long ballistic trajectories much larger than the simulation region.

In the results presented here the crater has a diameter of 200 m and maximum depth of 50 m. This crater size is consistent with observations of ponds on Eros, which are typically found in craters 20–300 m in diameter (Veverka et al., 2001; Robinson et al., 2001). The crater is also larger than the Debye length, so the photoelectron layer should roughly follow the contour of the topography. When the Sun is above the horizon a uniform photoelectron sheath is generated above the surface. At small values of i_s the solar wind plasma plays an important role in the sheath characteristics and our assumptions are not valid. We restrict our simulations to values of $i_s > 10°$. Shadowed regions are calculated based on the topography, and the sheath is assumed to be absent where there is a shadow. Although particles remain positively charged due to photoemission when over a shadowed part of the surface, there is no electric field generated by a photoelectron layer in the shadow to act on the charged particles. Particles then fall toward the shadowed region of the surface. If the particle horizontal velocity carries it across the shadowed region before it hits the surface the particle may return to being levitated in the photoelectron layer. Transport of dust into the shadowed region thus depends on the combination of the horizontal velocity and the size of the crater.

We place our model craters on the equator so that the Sun reaches the zenith at noon of each simulation day. This assumption reduces the amount of dust transport, which occurs preferentially at shadow boundaries. Sample trajectories with the Sun 20° above the horizon are shown in Fig. 6 with a particle transported into the shadowed region of the crater.

4. Results

4.1. Diurnal effects

We first test the simulation for edge effects and for the effects of topography with no electric force. The distribution of landing positions for a simulation with uncharged particles launched at speeds between 50 and 150 cm/s with $\alpha_0 = 80°$ is shown in Fig. 7. The tapering and sharp spikes at the limits of the surface are due to an edge effect: particles are launched outward beyond the range of the surface while none are launched from outside of the surface inward. Eight particles are launched from each of the 100 horizontal posi-
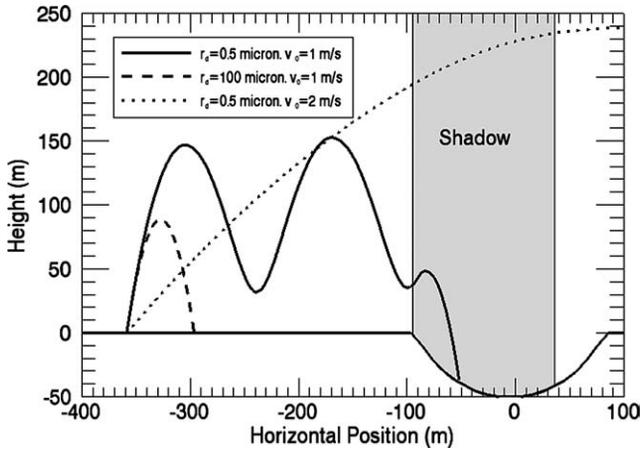
yicar7523

Fig. 6. (Solid) 0.5 μm particle launched at 100 cm/s at an angle of 80°. (Dash) 100 μm particle on a purely ballistic trajectory, launched at 100 cm/s at an angle of 80°. (Dot) 0.5 μm particle launched at 200 cm/s at an angle of 45°. The Sun is 20° above the left horizon.
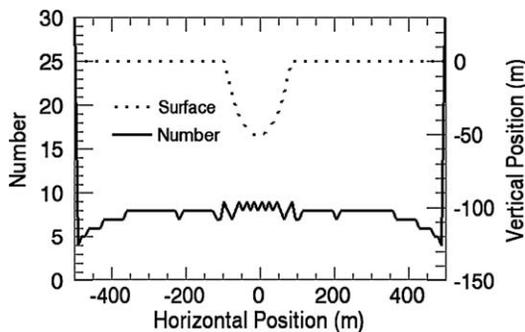

Fig. 7. Dust distribution with no photoelectron layer, showing the edge effects of the simulation and small variations introduced by the presence of topography.

Fig. 8. Dust distributions at fixed solar elevation angles from 10° to 40° above the horizon. The Sun is on the left of the image. Particles are 0.5 μm in radius and were launched from the surface at 50–150 cm/s at an angle of 80° to the horizontal. At higher solar elevation angles there is no shadow and all particles with these velocities and particle size remain levitated.

tions, four in each direction. The velocity range was chosen to match the velocities of particles that are levitated in the photoelectron layer. The effect of topography on the landing positions is small. When there is no sheath dust particles follow ballistic trajectories and are evenly distributed across the surface. When a sheath is imposed above the surface, the dust is no longer evenly distributed due to dust-sheath interactions.

We next consider the distribution of dust for the case where i_s is held constant. For this case, dust distributions are shown in Fig. 8 on the simulated Eros surface for solar incidence angles $i_s = 10°$ to $40°$. The simulation was run with the Sun at a fixed elevation until all particles hit the surface or the maximum time was reached. We use a maximum time of one half of an Eros rotation, or about 10^4 s. These simulations with a constant i_s illustrate the connection between shadow location and the landing positions of dust particles. No particles are launched from the shadowed part of the surface to simulate electrostatic levitation as the cause of the particle initially leaving the surface. We will discuss impact ejecta as well as electrostatic levitation as means of injecting dust into the photoelectron layer below. For the dust parti-
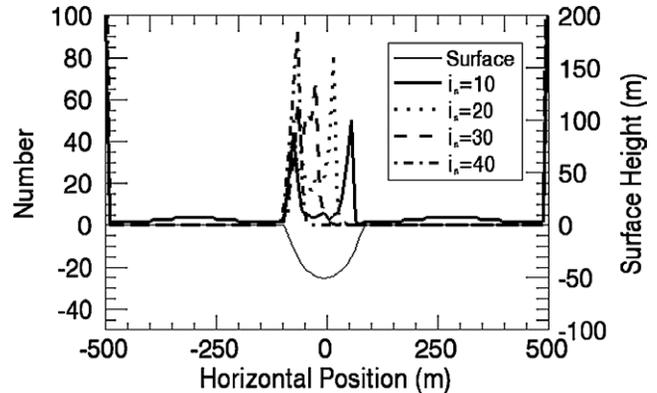
cles in Fig. 8 ($r_d = 0.5$ μm, $v_0 = 50–150$ cm/s), once the Sun is high enough to fully illuminate the crater, all particles remain levitated in the photoelectron layer throughout the simulation. At the lowest solar incidence angle ($i_s = 10°$), the fastest particles in the simulation pass through the photoelectron layer and hit the surface. At higher values of i_s all particles remain levitated except when they are over the shadowed region. The U-shaped profile of the dust distribution in the crater at the lower values of i_s in Fig. 8 represent the pile-up of dust at the shadow boundary: as soon as the particle enters the shadowed region it falls to the surface. This is partly an artifact of our simplified treatment of the photoelectron layer characteristics at a shadow boundary, where we ignore diffusion and simply turn off the photoelectron layer in the shadowed regions.

Next we simulate dust transport over an entire day of solar exposure on Eros by launching particles just after sunrise and calculating their trajectories while the Sun moves from $i_s = 10°$ to $180°$ in $2°$ steps at the rotation rate of Eros, or until the particle hits the surface. When the Sun is low on the horizon the levitation height is lower than at local noon. As the Sun rises, therefore, levitating particles rise as the photoelectron layer expands. Values of v_0 which result in levitation are also lower at small values of i_s because there is less distance for the photoelectron layer to decelerate particles descending through the layer. The particle launched at 1 m/s in Fig. 9 is suspended when the Sun is overhead, but not when the Sun is low on the horizon. The slower particles are suspended, and their trajectories are altered as they pass over the shadowed region of the crater. The levitation height also dips over the crater because the photoelectron layer follows the surface topography. One particle falls into the crater, while the other traverses the shadowed region and ultimately hits the surface at sunset. A dust distribution for a range of particle sizes and launch velocities is shown in Fig. 10 for a rotating Eros. Here we see a net accumulation of dust in the crater, but preferentially at the edges of the
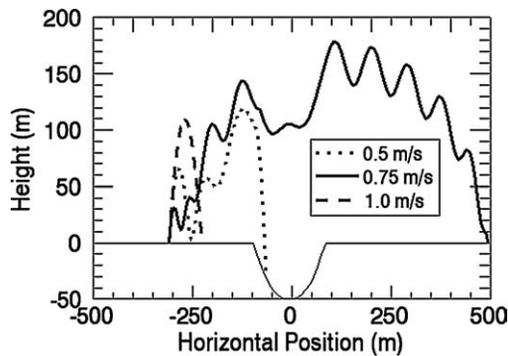
8   *J.E. Colwell et al. / Icarus ●●● (●●●●) ●●●–●●●*

Fig. 9. Trajectories of three 0.5 μm radius particles launched from the surface shortly after sunrise ($i_s = 10°$) with a rotation period equal to that of Eros. As the Sun rises the photoelectron layer expands (Fig. 2) and the particle levitates at a higher altitude above the surface (solid line). The dip of the solid particle over the crater reflects the fact that the photoelectron layer follows the topography in our model. The particle launched at 50 cm/s from the surface (dotted line) reaches the crater edge while it is still in shadow and falls to the surface.
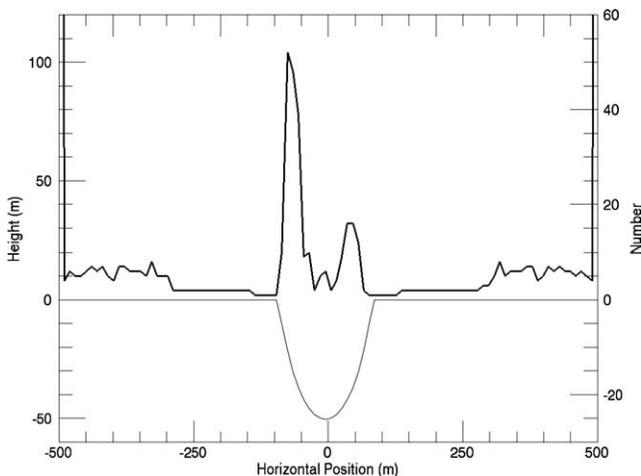

Fig. 10. Distribution of dust (thick line) for a simulation of an Eros day with dust particle radii $r_d = 0.3$ to 0.6 μm and $v_0 = 50–75$ cm/s. The simulated surface profile is shown in the thin line. Dust accumulates preferentially on the morning (left) side of the crater as it crosses over the shadow in the crater.

crater rather than center, as was seen with the simulations for a fixed value of i_s (Fig. 8).

4.2. Pond formation on Eros

The preceding sections illustrate the basic mechanism that dust levitation in a photoelectron sheath can lead to net transport of dust into a crater or other shadowed depression. Small dust particles levitated by the near surface electric field generated by photoemission from the surface may be transported into shadowed regions where the photoelectron layer is absent or greatly diminished. The details of the resulting dust distributions are dependent on a number of unknown parameters, such as the angle and speed that particles initially lift off the surface, the interactions between charged particles in the photoelectron layer that can also

lead to horizontal transport, and the work function of the asteroidal material. Electrostatic levitation provides a mechanism to transport dust into shadowed regions, including craters. This is not sufficient to explain the smooth, flat pond deposits observed on Eros, but it may indicate that electrostatic levitation and transport of dust works in concert with other mechanisms such as impact-induced seismic shaking (Cheng et al., 2002).

In order for electrostatic transport to play an important role in pond formation the process must occur on a short enough time scale. The net redistribution of regolith due to electrostatic transport processes near the surface is dependent on the rate particles are launched from the surface. This value is difficult to determine. Two mechanisms can allow particles to overcome the cohesion forces and gravity binding them to the surface: an electrostatic force or a mechanical disturbance (such as a micrometeoroid impact). It is unlikely that ponds are formed by dust launched off of the surface due to micrometeoroid bombardment (see Section 4.3.1). However, we have observed electrostatic launching of dust particles tens of μm in size in our laboratory experiments at 1 g (Sickafoose et al., 2002; Robertson et al., 2003). For the smaller, μm-sized particles discussed here, the surface cohesion forces between particles dominate the weak gravitational force on Eros. Particles are most likely to be electrostatically released from the surface at the terminator region, where the electric fields are orders of magnitude larger than at other locations on the surface (Criswell and De, 1977). For this reason, the above numerical simulations were performed with all particles launching across the surface at sunrise.

Particles launching at sunset are neglected because there is no photoelectron sheath on the nighttime side, and in this paper we do not model the nighttime solar wind plasma sheath. Because of this assumption particles tend to accumulate more on the morning side of the crater in our simulations. If particles launch at terminator regions, it is also possible that they can launch at shadow/light interfaces caused by crater topography. This situation can lead to redistribution of dust within the crater, perhaps enhancing the formation of ponds from dust transported into a crater from the exterior.

4.3. Timescale for pond formation

In order to produce the observed pond deposits we next consider the rate of transport and the timescale for pond formation. A full simulation of the regolith on Eros is beyond the scope of this paper; the following is a simple order-of-magnitude estimate of the rate of electrostatic transport to determine if it is capable of supplying enough material to produce the observed deposits in Eros craters. Our simulations artificially inject particles into the sheath at prescribed velocities and at a prescribed rate. The actual rate of particle levitation or ejection from the surface is unknown, but we can make estimates based on two physical mechanisms for launching dust off the surface.

ARTICLE IN PRESS

S0019-1035(04)00384-7/FLA AID:7523 Vol.●●●(●●●)   yicar7523   [DTD5] P.9(1-11)
YICAR:m5 v 1.35 Prn:22/02/2005; 9:54   by:Rima p. 9

Electrostatic dust transport on Eros   9

4.3.1. Meteoroid bombardment

The surface of Eros is bombarded by interplanetary micrometeoroids which eject particles from the surface on impact. The number of particles ejected off the surface of Eros that may be transported into a crater via electrostatic levitation is

$$N_{\text{ejecta}} = F_{\text{micro}} Y f_{\text{size}} f_{\text{velocity}} / M_{\text{particle}}, \quad (13)$$

where $F_{\text{micro}} \approx 10^{-16}$ g/(cm^2 s) (e.g., Grün et al., 1985), $Y \sim 10^5$ is a typical yield for a hypervelocity impact into regolith (Colwell and Esposito, 1990), f_{size} and f_{velocity} are the mass fractions of ejecta in the size and velocity ranges that lead to electrostatic transport, and M_{particle} is the mass of a dust grain. We find particles smaller than 1 µm are transported into the shadowed regions, and the fraction of ejecta that can be transported in this way is thus

$$f_{\text{size}} \leqslant \frac{\int_{r_1}^{1} m(r) n(r)\, dr}{\int_{r_1}^{r_{\text{max}}} m(r) n(r)\, dr} \approx \frac{\sqrt{1} - \sqrt{r_1}}{\sqrt{r_{\text{max}}}} \approx 0.01, \quad (14)$$

where we have assumed the ejecta size distribution $n(r)\, dr \sim r^{-3.5}\, dr$, $r_1 \ll 1$ µm, and $r_{\text{max}} \sim 1$ cm is the largest particle ejected by a typical micrometeoroid of radius 500 µm with a yield of $Y = 10^5$. The value in Eq. (14) is an upper limit because the size distribution of dust on Eros may be falling off at such small particle sizes. Similarly, the mass fraction of ejecta in the velocity range, $v = v_1$ to v_2, that allows for levitation and horizontal transport, is

$$f_{\text{velocity}} = \left(\frac{v_1}{v_{\text{min}}}\right)^{-1.2} - \left(\frac{v_2}{v_{\text{min}}}\right)^{-1.2} = 0.85, \quad (15)$$

where we assume that $v_{\text{min}} \leqslant v_1$, $v_1 = 25$ cm/s, $v_2 = 125$ cm/s, and the power-law index of the velocity mass distribution is for impacts into regolith (Housen et al., 1983). Compensating for the large value of α_0 adopted for the numerical simulations to $\alpha_0 = 45$, more appropriate for impact ejecta, increases the values of v_1 and v_2 that lead to levitation, but does not significantly affect the value of f_{velocity}. The result is $N_{\text{ejecta}} = 2 \times 10^{-4}$ cm^{-2} s^{-1}. Because our simulations have a 1D surface, we assume $r_d = 1$ µm and get a 1D injection rate of $N_{\text{ejecta}} = 3 \times 10^{-8}$ cm^{-1} s^{-1} or 30 particles per linear km per Eros day.

Because the enhancement of crater dust that we find is dependent on the particular values of particle sizes and launch speeds as well as the dimension of the crater it is not possible to determine a precise rate of dust transport into the crater. Nevertheless, our simulations provide an order-of-magnitude estimate of the rate of dust transport. In a simulation with $v_0 = 25$–100 cm/s and $r_d = 0.1$–1.0 µm, the enhancement of dust in the crater compared to the surrounding terrain in our simulations is 10 particles per 10-m linear element per Eros day, where the total number of particles launched in the simulation was 6257. Most particles in this simulation went beyond the simulation boundaries before landing. In a simulation with only 0.5 µm particles at $v_0 = 50$ cm/s we find 1.6 particles per 10-m linear element in

the crater where the total number of particles launched was 168 and again most particles were transported beyond the simulation boundaries. The larger fraction of particles transported to the crater for the single size simulation (1.6/168 vs. 10/6257) simply reflects the fact that the largest particles in the bigger simulation are not levitated and the smaller particles are levitated higher and are therefore less likely to fall into the shadowed crater. In order to estimate a lower limit for the time scale for pond formation via micrometeoroid ejecta loading the photoelectron layer, we use the higher rate we find from the optimal values of $r_d = 0.5$ µm and $v_0 = 50$ cm/s. We therefore scale the result of 1.6 particles per 10-m element per day by the factor of 30/168 representing the estimated ratio of ejecta particles in the relevant size range to the number launched in the simulation. This gives 0.3 particles per 10-m element per Eros day or 1 monolayer of micron-sized particles in 3×10^6 Eros days and 3×10^{12} Eros days or $\sim 2 \times 10^9$ years to build up an extra meter of dust inside the crater.

Micrometeoroid ejecta therefore seems an unlikely source of dust for pond formation via electrostatic transport. This is consistent with observations of dust levitated over the lunar horizon (Rennilson and Criswell, 1974) and horizon glow observed by the Clementine spacecraft and Apollo astronauts (Zook et al., 1995) implying a much greater abundance of dust leaving the surface than can be accounted for by micrometeoroid bombardment.

4.3.2. Electrostatic levitation

Electrostatic levitation of dust off the surface may therefore provide enough charged dust in the photoelectron layer to lead to formation of the observed pond features if it acts as efficiently on Eros as it apparently does on the Moon. We can make crude estimates of the launch rate by electrostatic levitation, though there are several uncertainties: the strength of the binding force between particles, the strength of the electric field at the surface of Eros, and the photoelectric yield of the particles.

If the electric force is sufficient to levitate particles in the relevant size range, then there could be one monolayer of µm-sized particles injected into the photoelectron layer each day. We can make a set of assumptions about this process to test whether it is plausible for this to lead to pond formation. The area fraction of the monolayer of levitated particles depends on the size distribution of particles in the regolith and the distribution of regolith on the surface. Assuming that this fraction is high enough so that when combined with the enhancement of dust inside the crater compared to outside from our numerical simulations, then there is a net addition of one monolayer in the forming pond each Eros day and the pond formation timescale is only ~ 2000 years. Lee (1996) similarly concludes that electrostatic levitation occurs more rapidly than production of small particles by micrometeoroid bombardment.

A third indication that the rate of levitation is sufficient to lead to pond formation, following the lunar observations

and Lee's charging timescale, comes from our laboratory experiments. We observe dust to spontaneously lift off of a surface having a plasma sheath (plasma conditions are those described in Robertson et al. (2003), and the plate is biased to −100 V). Experimentally, we have observed particles to launch from a graphite plate with a crater-like depression surrounded by a plasma sheath at a rate of approximately 1 per cm per second, looking at a 1 cm-wide section of our plate with a shallow (≪ 1 cm) depth of focus. The daytime global surface potential of Eros is likely much smaller, on the order of ∼ 5 V (Section 2), but terminator fields may be much higher than the 100 V potential in the laboratory experiment (e.g., 550–1000 V/cm in Criswell (1972, 1973); 100–1000 V/cm in Pelizzari and Criswell (1978), though the potential difference is over a short spatial scale so that at no time was any potential more than twice the electron energy). The weight of the particles is also much higher in the laboratory than on Eros, but the cohesive forces may be less since we levitated larger particles (with a smaller surface area to mass ratio) from a thin layer instead of from a thick regolith. If we ignore the admittedly large uncertainties due to these differences, then the electrostatic levitation rate is $N_{\text{electrostatic}} \sim 1 \text{ cm}^{-1}\text{s}^{-1}$. This rate is $\sim 2 \times 10^7$ times N_{ejecta} and gives a correspondingly shorter timescale for pond formation of $\sim 10^2$ years. The only conclusion we draw from these two rough estimates is that neither argument rules out electrostatic levitation as a viable mechanism for pond formation on Eros.

5. Discussion and conclusions

A numerical model of dust levitation and transport in a photoelectron sheath above the surface of Eros demonstrates that particles smaller than 1 μm tend to collect in craters and regions of shadow. Over the course of a day, dust is primarily transported into a crater and is redistributed over the flat portions of the surface. These simulations support the idea that features like the dust ponds observed by the NEAR-Shoemaker spacecraft at Eros may be caused by electrostatic dust transport. In particular, we find:

- particles smaller than ~ 1 μm in radius can be stably levitated in the photoelectron sheath on Eros at a height of tens to hundreds of meters, depending on the particle size and time of day;
- particles smaller than ~ 1 μm knocked off the surface at speeds exceeding a few tens of cm/s are accelerated upward by the photoelectron layer electric field where they are subject to long range transport in the layer as well as potential loss from the asteroid;
- there is a net transport of dust in the photoelectron layer to shadowed regions, such as craters;
- injection of dust into the photoelectron layer by electrostatic levitation off the surface can occur fast enough to

transport enough dust into craters to create the Eros dust ponds.

Our simulations do not, however, reproduce the Eros dust ponds in detail. We find an accumulation of dust near the edges of craters, rather than a central smooth deposit. The detailed shape of our dust distribution is controlled by factors such as the initial horizontal velocity, the path of the shadow boundary over the course of a day, the size and velocity distributions of levitated particles, and the behavior of the photoelectron layer at the light/shadow boundary as a function of height above the surface. We have assumed an abrupt boundary which naturally leads to an enhanced concentration of dust at that boundary.

More detailed calculations are needed to address the long term evolution of the dust distribution on Eros, including processes other than just electrostatic levitation. In this first study we have focused only on the dayside electrostatic transport of dust, but strong terminator fields as well as a solar wind plasma sheath on the night side may play an important role in the dynamics of charged dust on asteroids such as Eros. A correlation between diurnal sunlight and shadow patterns and the distribution of ponds on Eros would support the hypothesis that photoelectric levitation plays a role in their formation.

Acknowledgment

References

Arnas, C., Mikikian, M., Doveil, F., 1999. High negative charge of dust particles in a hot cathode discharge. Phys. Rev. E 60, 7420–7425.

Berg, O.E., Richardson, F.F., Rhee, J.W., Auer, S., 1974. Preliminary results of a cosmic dust experiment on the Moon. Geophys. Res. Lett. 1, 289–290.

Berg, O.E., Wolf, H., Rhee, J., 1976. Lunar soil movement registered by the Apollo 17 cosmic dust experiment. In: Elsässer, H., Fechtig, H. (Eds.), Interplanetary Dust and Zodiacal Light. Springer-Verlag, Heidelberg, pp. 233–237.

Cheng, A.F., Barnouin-Jha, O., Zuber, M.T., Veverka, J., Smith, D.E., Neumann, G.A., Robinson, M., Thomas, P., Garvin, J.B., Murchie, S., Chapman, C., Prockter, L., 2001. Laser altimetry of small-scale features on 433 Eros from NEAR-Shoemaker. Science 292, 488–491.

Cheng, A.F., Izenberg, N., Chapman, C.R., Zuber, M.T., 2002. Ponded deposits on Asteroid 433 Eros. Meteorit. Planet. Sci. 37, 1095–1105.

Colwell, J.E., Esposito, L.W., 1990. A numerical model of the uranian dust rings. Icarus 86, 530–560.

Criswell, D.R., 1972. Lunar dust motion. Proc. Lunar Sci. Conf. 3, 2671–2680.

Criswell, D.R., 1973. Horizon-glow and the motion of lunar dust. In: Grard, R.J.L. (Ed.), Photon and Particle Interactions with Surfaces in Space. Reidel, Dordrecht, pp. 545–556.

Criswell, D.R., De, B.R., 1977. Intense localized photoelectric charging in the lunar sunset terminator region. 2. Supercharging at the progression of sunset. J. Geophys. Res. 82, 1005–1007.

Doe, S.J., Burns, O., Pettit, D., Blacic, J., Keaton, P.W., 1994. The levitation of lunar dust via electrostatic forces. In: Galloway, R.G., Lokaj, S. (Eds.), Engineering, Construction, and Operations in Space. American Society of Civil Engineers, New York, pp. 907–915.

Goertz, C.K., 1989. Dusty plasmas in the Solar System. Rev. Geophys. 27 (2), 271–292.

Gold, T., 1955. The lunar surface. Mon. Not. R. Astron. Soc. 115, 585–604.

Grard, R.J.L., Tunaley, J.K.E., 1971. Photoelectron sheath near a planetary probe in interplanetary space. J. Geophys. Res. 76, 2498–2505.

Grün, E., Zook, H.A., Fechtig, H., Giese, R.H., 1985. Collisional balance of the meteoritic complex. Icarus 62, 244–272.

Havnes, O., Goertz, C.K., Morfill, G.E., Grün, E., Ip, W., 1987. Dust charges, cloud potential, and instabilities in a dust cloud embedded in a plasma. J. Geophys. Res. 92, 2281–2287.

Housen, K.R., Schmidt, R.M., Holsapple, K.A., 1983. Crater ejection scaling laws: fundamental forms based on dimensional analysis. J. Geophys. Res. 88, 2485–2499.

Ip, W.H., 1986. Electrostatic charging and dust transport at Mercury's surface. Geophys. Res. Lett. 13, 1133–1136.

Kareev, M.S., Sears, D.W.G., Benoit, P.H., Thompson, J., Jansma, P., Mattioli, G., 2002. Laboratory simulation experiments and the ponds on Asteroid 433 Eros. Lunar Planet. Sci. 33. Abstract 1610.

Kerr, R.A., 2001. Strange doings on a NEAR-struck asteroid. Science 291, 1467–1469.

Lee, P., 1996. Dust levitation on asteroids. Icarus 124, 181–194.

McCoy, J.E., Criswell, D.R., 1973. Evidence for a high altitude distribution of lunar dust. Proc. Lunar Sci. Conf. 5, 496–497.

Mendis, D.A., Hill, J.R., Houpis, H.L.F., Whipple Jr., E.C., 1981. On the electrostatic charging of the cometary nucleus. Astrophys. J. 249, 787–797.

Nitter, T., Aslaksen, T.K., Melandsø, F., Havnes, O., 1994. Levitation and dynamics of a collection of dust particles in a fully ionized plasma sheath. IEEE Trans. Plasma Sci. 22, 159–172.

Nitter, T., Havnes, O., Melandsø, F., 1998. Levitation and dynamics of charged dust in the photoelectron sheath above surfaces in space. J. Geophys. Res. 103, 6605–6620.

Pelizzari, M.A., Criswell, D.R., 1978. Lunar dust transport by photoelectric charging at sunset. Proc. Lunar Sci. Conf. 9, 3225–3237.

Pieters, C.M., 2001. Regolith processes on Eros. AGU (Fall meeting). Abstract #P32B-0558.

Rennilson, J.J., Criswell, D.R., 1974. Surveyor observations of lunar horizon glow. The Moon 10, 121–142.

Robertson, S., Gulbis, A.A.S., Colwell, J., Horányi, M., 2003. Dust grain charging and levitation in a weakly collisional sheath. Phys. Plasmas 10, 3874–3880.

Robinson, M.S., Thomas, P.C., Veverka, J., Murchie, S., Carcich, B., 2001. The nature of ponded deposits on Eros. Nature 413, 396–400.

Sickafoose, A.A., Colwell, J.E., Horányi, M., Robertson, S., 2001. Experimental investigations on photoelectric and triboelectric charging of dust. J. Geophys. Res. 106 (A5), 8343–8356.

Sickafoose, A.A., Colwell, J.E., Horány, M., Robertson, S., 2002. Experimental levitation of dust grains in a plasma sheath. J. Geophys. Res. 107.

Sternovsky, Z., Sickafoose, A.A., Colwell, J.E., Robertson, S., Horányi, M., 2002. Contact charging of lunar and martian dust simulants. J. Geophys. Res. 107 (E11).

Tepliczky, I., Kereszturi, A., 2002. Signs of change in the electrostatic sedimentation of Eros. Lunar Planet. Sci. 33. Abstract 1656.

Veverka, J., 32 colleagues, 2000. NEAR at Eros: imaging and spectral results. Science 289, 2088–2097.

Veverka, J., 32 colleagues, 2001. Imaging of small-scale features on 433 Eros from NEAR: evidence for a complex regolith. Science 292, 484–488.

Willis, R.F., Anderegg, M., Feuerbacher, B., Fitton, B., 1973. Photoemission and secondary electron emission from lunar surface material. In: Gard, R. (Ed.), Photon and Particle Interaction with Surfaces in Space. Reidel, Dordrecht, pp. 369–387.

Zook, H.A., McCoy, J.E., 1991. Large-scale lunar horizon glow and a high altitude lunar dust exosphere. Geophys. Res. Lett. 18, 2117–2120.

Zook, H.A., Potter, A.E., Cooper, B.L., 1995. The lunar dust exosphere and Clementine lunar horizon glow. Lunar Planet. Sci. 26, 1577–1578.